somewhat slower) mixing for spatially periodic forcing; (4) for temporally non-periodic forcing, there are no recurrences.

The one-dimensional spatial power spectrum $E(k)$ computed in the standard way[10] provides a useful diagnostic for the development of fine structure in the concentration field. An example is shown in Fig. 4a for time-periodic forcing using the spatially disordered magnet array (as in Fig. 2), at several different times. For $l < t < 10$, the high frequency tail of $E(k)$ rises, as stretching and folding produce fine structure. Later, the entire spectrum declines at all frequencies with little further change of shape. The decline at high k is due to diffusion, and the decline at low k is due to the continuing transport of spectral variance to high k by stretching. The spectrum does not follow a well-defined power law (nor is one expected[6] for transient mixing); it is steeper at higher k. The behaviour of the second spectral moment $\langle k^2 \rangle$, shown in Fig. 4b, increases rapidly at first and then essentially saturates, consistent with the asymptotic structure noted earlier.

The fine structure of the dye pattern may also be investigated by studying the PDF of the magnitude of the concentration gradient. An example is shown in Fig. 5 for the same conditions as in Fig. 2. Gradients have been expressed in units of the standard deviation of the concentration field to compensate for the gradual homogenization. It is striking to see that the gradient PDF reaches an invariant form that is essentially identical at $t = 20$ and 50 periods. The distribution at high gradients is accurately exponential. Such exponential tails for distributions of concentration gradients have been noted in several theoretical studies[13]. When the same experiment is done for the weakly turbulent flow at lower viscosity, the resulting distribution is similar to that of Fig. 5 for $t = 10$, but the shape continues to evolve, approaching a maxwellian distribution (characteristic of independent gaussian components) at longer times. Therefore, the large gradients are attenuated more rapidly than are small gradients for the turbulent flow. Diffusion broadens the striations in two-dimensional turbulence, but not in chaotic mixing.

We find that chaotic mixing, produced by time-periodic cellular flows, leads to a remarkable persistent spatial structure, a complex pattern that recurs periodically while its contrast decays slowly with time. The recurrence is surprising (when first encountered) since additional striations are created during each cycle. The corresponding spatial power spectrum retains its shape as it declines simultaneously at all wavenumbers owing to a delicate balance of two distinct processes: stretching and diffusion. The probability distribution of the magnitude of the concentration gradient reaches an invariant form (when suitably normalized) with a peak at non-zero gradient and exponential tails. All of these properties show that the recurrent mixing pattern represents a dynamical non-equilibrium state rather than a static condition. Finally, we note that identically forced but weakly turbulent flows at lower viscosity become homogeneous and transport material much more rapidly than the time-periodic flows manifesting chaotic advection. However, turbulence is generally unavailable when mixing in small scale devices is required. □

Received 3 June; accepted 18 August 1999.

1. Aref, H. Stirring by chaotic advection. *J. Fluid Mech.* **143,** 1–21 (1984).
2. Ottino, J. M. Mixing, chaotic advection, and turbulence. *Annu. Rev. Fluid Mech.* **22,** 207–253 (1990).
3. Fountain, G. O., Khakhar, D. V. & Ottino, J. M. Visualization of three-dimensional chaos. *Science* **281,** 683–686 (1998).
4. Pierrehumbert, R. T. Tracer microstructure in the large-eddy dominated regime. *Chaos Solitons Fractals* **4,** 1091–1110 (1994).
5. Antonsen, T. M., Fan, Z., Ott, E. & Garcia-Lopez, E. The role of chaotic orbits in the determination of power spectra of passive scalars. *Phys. Fluids* **8,** 3094–3104 (1996).
6. Antonsen, T. M. & Ott, E. Multifractal power spectra of passive scalars convected by chaotic fluid flows. *Phys. Rev. A* **44,** 851–857 (1991).
7. Muzzio, F. J., Meneveau, C., Swanson, P. D. & Ottino, J. M. Scaling and multifractal properties of mixing in chaotic flows. *Phys. Fluids A* **4,** 1439–1456 (1992).
8. Alvarez, M. M., Muzzio, F. J., Cerbelli, S., Adrover, A. & Giona, M. Self-similar spatiotemporal structure of intermaterial boundaries in chaotic flows. *Phys. Rev. Lett.* **81,** 3395–3398 (1998).
9. Paret, J., Marteau, D., Paireau, O. & Tabeling, P. Are flows electromagnetically forced in thin stratified layers two-dimensional? *Phys. Fluids* **9,** 3102–3104 (1997).
10. Williams, B. S., Marteau, D. & Gollub, J. P. Mixing of a passive scalar in two-dimensional turbulence. *Phys. Fluids* **9,** 2061–2080 (1997).
11. Paret, J. & Tabeling, P. Experimental observation of the two-dimensional inverse energy cascade. *Phys. Rev. Lett.* **79,** 4162–4165 (1997).
12. Miller, P. L. & Dimotakis, P. E. Reynolds number dependence of scalar fluctuations in a high Schmidt number turbulent jet. *Phys. Fluids A* **3,** 1156–1163 (1991).
13. Shraiman, B. I. & Siggia, E. D. Lagrangian path integrals and fluctuations in random flow. *Phys. Rev. E* **49,** 2912–2927 (1994).

Acknowledgements

We thank J. Andersen, J.-C. Geminard, A. Kudrolli, and W. Losert for experimental contributions, and E. Ott and B. Shraiman for discussions. This work was supported by the Condensed Matter Physics Program of the US NSF.

Correspondence and requests for materials should be addressed to J.P.G. (e-mail: jgollub@haverford.edu).

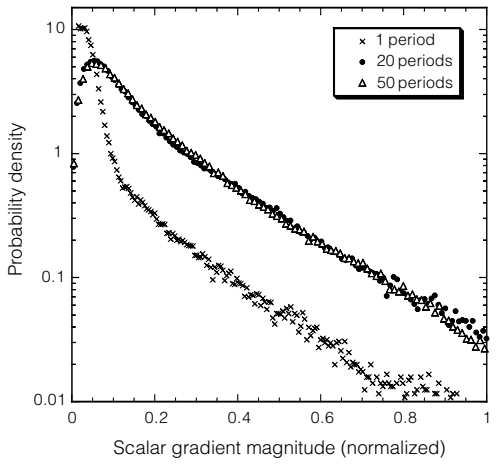

Figure 5 Probability distribution of the magnitude of the concentration gradient for chaotic mixing (Fig. 2). The distribution, here normalized by the standard deviation of the intensity field to compensate for the gradual loss of contrast, reaches an invariant form after about 20 periods, with a peak at finite gradient and an exponential tail.

Sonoluminescence temperatures during multi-bubble cavitation

William B. McNamara III*, Yuri T. Didenko*‡ & Kenneth S. Suslick*

* *Department of Chemistry, University of Illinois at Urbana-Champaign, 600 S. Mathews Avenue, Urbana, Illinois 61801, USA*

Acoustic cavitation—the formation and implosive collapse of bubbles—occurs when a liquid is exposed to intense sound. Cavitation can produce white noise, sonochemical reactions, erosion of hard materials, rupture of living cells and the emission of light, or sonoluminescence[1,2]. The concentration of energy during the collapse is enormous: the energy of an emitted photon can exceed the energy density of the sound field by about twelve orders of magnitude[3], and it has long been predicted that the interior bubble temperature reaches thousands of degrees Kelvin during collapse. But experimental measurements[4,5] of

‡ Permanent address: Pacific Oceanological Institute, Vladivostok 690061, Russia.

conditions inside cavitating bubbles are scarce, and there have been no studies of interior temperature as a function of experimental parameters. Here we use multi-bubble sonoluminescence from excited states of metal atoms as a spectroscopic probe of temperatures inside cavitating bubbles. The intense atomic emission allows us to change the properties of the gas–vapour mixture within the bubble, and thus vary the effective emission temperature for multi-bubble sonoluminescence from 5,100 to 2,300 K. We observe emission temperatures that are in accord with those expected from compressional heating during cavitation.

We previously discovered that sonication of solutions of $Fe(CO)_5$, $Cr(CO)_6$ and $Mo(CO)_6$ produced multi-bubble sonoluminescence (MBSL) spectra from excited states of iron, chromium, and molybdenum atoms[6]. Improved spectral resolution now enables us to use these emissions to determine effective temperatures for the emitting excited states. As an example, calculated and observed spectra for Cr under Ar at 20 kHz are given in Fig. 1; the synthetic spectra are generated using the theory of atomic emission[7]. Analogous spectra were also collected for Mo and Fe in order to test the validity of this method. The relative integrated intensities (I_1/I_2) of two atomic lines emitted from the different excited states of the same metal atom are given by equation (1):

$$\frac{I_1}{I_2} = \frac{g_1 A_1 \lambda_2}{g_2 A_2 \lambda_1} \exp[(E_1 - E_2)/kT_e] \quad (1)$$

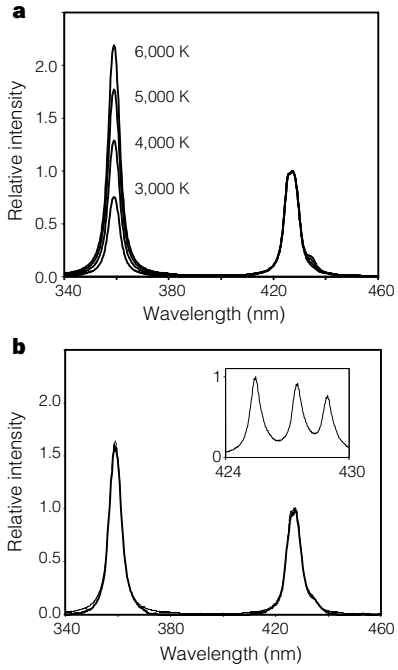

Figure 1 Multi-bubble sonoluminescence (MBSL) emission from excited states of Cr atoms. **a**, Calculated spectra as a function of temperature. **b**, The observed emission spectrum compared to the best-fit calculated spectrum (4,700 K). Inset, observed spectrum at higher resolution, which resolves the individual atomic emission lines. Sonoluminescence was generated from 2.5 mM solutions of metal carbonyls (0.25 mM for $Mo(CO)_6$ due to solution absorbance) in poly(dimethylsiloxane) (Dow 200 silicone oil, 100 centistokes viscosity) irradiated at ~90 W cm^{-2} at 20 kHz (Heat Systems Mysonix 375, with 0.5 inch Ti horn), and spectra collected with an 0.5 m spectrograph (Acton Research 505F with a Princeton Instruments IRY 512N diode array). The solutions were continuously sparged with the appropriate gas during sonication, and each spectrum is the average of at least 15 10-second collections. All spectra were corrected for absorbance by the solution and for the response of the optical system. Imaging of the MBSL shows that the emission comes from a dense cloud of emitting bubbles rather than from a few exceptional ones.

where g is the degeneracy of the electronic state, A is the Einstein transition probability for the electronic transition, λ is the wavelength of the emitted line, E is the energy of the electronic state, and T_e is the electronic temperature. The transition probabilities, degeneracies, wavelengths, and excited-state energies were taken from the literature[8–10]. This technique has been well established for flame and plasma diagnostics[11,12], and is proving to be a versatile method of determining the effective temperature of cavitational bubble collapse under a variety of experimental conditions.

The temperatures from three different metal atomic line emissions yielded very consistent results. High-resolution spectra of the MBSL emission from Cr and Mo atoms were collected from solutions of the hexacarbonyl complexes of these metals (Fig. 1 inset). The relative intensity of each line within a given multiplet was measured from these spectra, and the relative intensity of each multiplet was then determined from lower-resolution spectra. This process allowed for a line by line comparison of relative intensities for these two metals across the entire spectral window. The temperatures were then determined by the use of atomic Boltzmann plots[13]: Cr and Mo atom emission temperatures were respectively 4,700 ± 300 K and 4,800 ± 400 K, under Ar at 20 kHz. The linearity of these plots also indicated that the emission is thermally equilibrated. The high resolution MBSL spectra of Fe emission are too complex to allow for the determination of individual line intensities, and the experimental spectra were therefore compared to synthetic spectra generated using equation (1), with an excellent fit to data found for a temperature of 5,100 ± 300 K.

We previously used two different techniques to measure the temperature of cavitation in Ar-saturated liquids. The first made use of sonochemical kinetics for a comparative rate thermometry analysis of the dissociation of CO from various metal carbonyls[5]. This technique is independent of sonoluminescence, and yielded an effective reaction temperature of 5,200 ± 500 K for the gas phase of cavitation under Ar. The second technique applied spectral analysis to C_2 emission bands in the MBSL from the sonication of silicone oil under Ar, giving an effective emission temperature of 5,075 ± 150 K (ref. 4). The temperatures reported here are in good agreement with these previously determined values. We note that the previous MBSL emission spectra of C_2 under similar conditions also appeared to be thermally equilibrated[4,14].

These metal-atom emissions are the most intense sonoluminescence yet observed. This allows us to study MBSL under conditions previously experimentally inaccessible. Multi-bubble sonoluminescence is generally believed to arise from compressional heating of the bubble contents during the final stage of bubble collapse. The intrabubble temperature should therefore depend on the properties

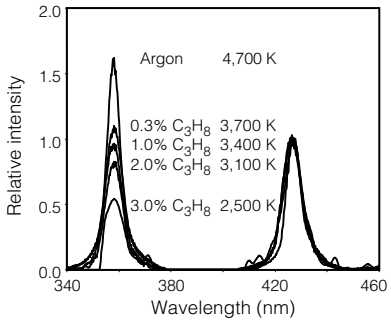

Figure 2 Effect of polyatomic gases on the observed emission temperatures from MBSL. The MBSL spectra are from solutions of $Cr(CO)_6$ in silicone oil, obtained as in Fig. 1. From top to bottom, the sparge gas was Ar mixed with 0.0, 0.3, 1.0, 2.0, and 3.0 vol % propane, yielding respective emission temperatures of 4,700 K, 3,700 K, 3,400 K, 3,100 K and 2,500 K.

of the gas and vapour mixture within the bubble, particularly the polytropic ratio ($\gamma = C_p/C_v$, ratio of heat capacities) and the thermal conductivity. The effect of each of these parameters was examined by collecting MBSL spectra from several liquids containing a variety of dissolved gases.

If emission results from compressional heating, the effective temperature and pressure reached during cavitation will drop as γ decreases (for a given compression ratio). This prediction was tested by collecting MBSL spectra from $Cr(CO)_6$ solutions that were saturated with Ar doped with low concentrations of various gaseous hydrocarbons (methane, ethane, ethylene and propane). These polyatomic molecules have much higher heat capacities than does Ar, particularly at temperatures sufficient to populate their excited-state vibrational modes. Note that the thermal conductivities of these mixtures vary by less than a factor of two relative to argon.

The observed emission temperature does indeed decrease substantially as the polyatomic gas content is increased. For example, as Ar is doped with increasing amounts (up to 3%) of propane (Fig. 2), the emission temperature progressively decreases from 4,700 K to 2,500 K. The low resolution of the Cr spectra was necessitated by the decreasing intensity of emission at the higher concentrations of hydrocarbons. The measured emission temperatures for Ar mixtures with various hydrocarbons (methane, ethane, ethylene and propane) are given in Fig. 3. In all instances, the temperature of MBSL decreases as the percentage of a given hydrocarbon is increased (that is, as the polytropic ratio of the gas within the bubble is decreased). Similar results were observed for Fe with methane.

The very simplest model for cavitation assumes adiabatic compression during bubble collapse[2,15]: a gas with a polytropic ratio γ, compressed from an initial radius R_i to a final radius R_f, with an initial temperature T_i, has a final temperature T_f according to equation (2):

$$T_f = T_i \left(\frac{R_i}{R_f}\right)^{3(\gamma-1)} \quad (2)$$

This equation includes no dynamics of bubble motion, and neglects all effects from thermal transport, solvent vapour pressure, and chemical reactions within the bubble. Furthermore, equation (2) assumes a temperature-independent γ; however, γ decreases substantially as excited vibrational states become fully populated and it decreases even more if chemical reactions occur. Nonetheless, as shown in Fig. 3, the data are fitted reasonably well by equation (2) for a compression ratio of 3.65. We calculated the temperatures and pressures during bubble collapse by finite difference using a temperature dependent γ, and can fit our data to within experimental error. Given the lack of dynamics and the failure to incorporate chemical reactions (whose endothermicity is not neglible compared to the compressional heating), more detailed modelling[16] will be required to give meaningful results.

The polytropic ratio of the bubble interior can also be varied by changing the identity and vapour pressure of the solvent. The solvent vapours behave in the same manner as the gaseous hydrocarbons described above: an increase in the solvent vapour pressure is equivalent to increasing the percentage of hydrocarbon gas and leads to similar drops in temperature. Both MBSL intensities[17–19] and sonochemical rates[20,21] decrease dramatically with solvent vapour pressure increases. We collected MBSL spectra at different bulk solution temperatures from solutions of $Cr(CO)_6$ under Ar in octanol, a low volatility liquid whose vapour pressure as a function of temperature is well documented[22]. The results in Fig. 4 are consistent with compressional heating of the bubble contents: the temperature of MBSL decreases as the vapour pressure increases. Similar results were observed using other long-chain alcohols and alkanes, and using helium instead of argon.

Several reports have shown that the total intensity of MBSL from solutions saturated with noble gases decreases as the thermal conductivity of the noble gas increases. This has generally been attributed to thermal transport during cavitation: compressional heating combined with limited thermal transport in a "quasi-adiabatic"

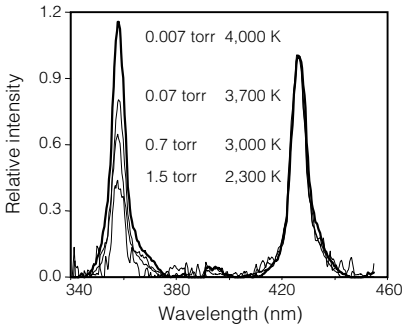

Figure 4 Effect of solvent vapour pressure on the observed emission temperatures from MBSL. The MBSL spectra are from solutions of $Cr(CO)_6$ in octanol, obtained as in Fig. 1. From top to bottom, the vapour pressure was 0.007, 0.07 and 1.5 torr, yielding emission temperatures of 4,000 K, 3,700 K, 3,000 K and 2,300 K, respectively.

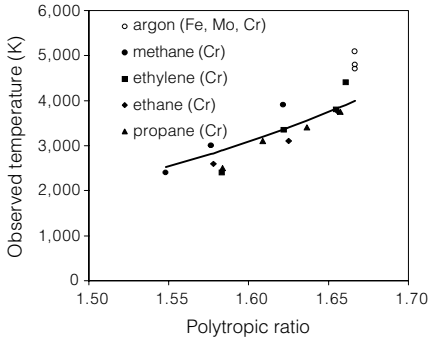

Figure 3 Observed emission temperatures versus gas-mixture polytropic ratios at 298 K. The polytropic ratio of heat capacities, γ, is given by C_p/C_v. The solid line is the best fit to simple adiabatic compression of a bubble with a radius ratio of 3.65, from equation (2); as γ is not temperature independent, equation (2) provides only an approximate model. The open circles give the observed emission temperatures from Fe, Mo, and Cr atom MBSL under argon; all other data are from Cr atom emission under given gases.

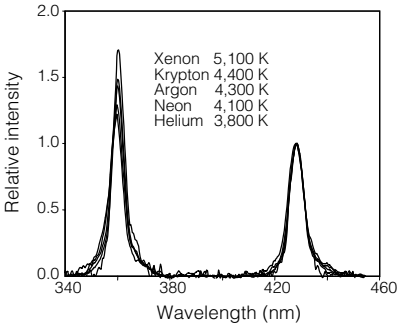

Figure 5 Effect of dissolved noble gases on the observed emission temperatures from MBSL. The MBSL spectra are from solutions of $Cr(CO)_6$ in octanol, obtained as in Fig. 1. From top to bottom, the dissolved gas was Xe, Kr, Ar, Ne and He, with respective emission temperatures of 5,100 K, 4,400 K, 4,300 K, 4,100 K and 3,800 K.

collapse[16,23–25]. The rate at which energy is transferred out of the bubble is expected to increase as the thermal conductivity of the gas within the bubble increases. Bubbles containing helium, therefore, should be cooler than bubbles containing argon or xenon, although the predicted extent of this effect is debatable[24]. In order to examine the importance of thermal conduction, MBSL spectra were obtained from solutions of $Cr(CO)_6$ in octanol saturated with different noble gases. The results in Fig. 5 show that the temperature of MBSL decreases as the thermal conductivity of the gas within the bubble increases. Similar results were observed using dodecane.

We note that the thermal conductivities of the noble gases used here span a factor of thirty, while the thermal conductivities of the argon and hydrocarbon mixtures differ by only a factor of two, therefore, the temperature changes observed upon the addition of hydrocarbons to argon are not due to changes in thermal conductivity.

We have shown that the observed emission temperature within imploding cavitation bubbles depends on both the polytropic ratio and the thermal conductivity of the bubble contents. The processes occurring within the bubble, however, are more complex than can be described by the simple physics of compressional heating. A cavitation bubble functions as a small chemical reactor, and so the identity of the bubble contents will change during bubble collapse. The sonolysis of organic liquids generates H_2 and C_2H_2 as well as other small hydrocarbons[20], and similar processes will occur during the sonolysis of silicone oil. Evidence for this is seen in the MBSL spectra: the spectra of all the systems described here contain features attributable to excited states of C_2 and CH (refs 4, 18, 26), and we also find that sonication of silicone oil leads to intense emission from excited Si atoms. These chemical processes can absorb large amounts of energy during the compression. Furthermore, if sufficient dissociation occurs, the sonolysis products (mostly diatomics and polyatomics) will substantially lower the polytropic ratio and increase the pressure inside the bubble. This makes it increasingly difficult to further compress and heat the bubble[27]. These factors will limit the temperatures achievable by compressional heating within cavitation bubbles. □

Received 4 May; accepted 23 August 1999.

1. Suslick, K. S. & Crum, L. A. in *Handbook of Acoustics* (ed. Crocker, M. J.) 243–253 (Wiley-Interscience, New York, 1998).
2. Knapp, R. T., Daily, J. W. & Hammitt, F. G. *Cavitation* (McGraw-Hill, New York, 1970).
3. Barber, B. P. & Putterman, S. J. Observation of synchronous picosecond sonoluminescence. *Nature* **352,** 318–320 (1991).
4. Flint, E. B. & Suslick, K. S. The temperature of cavitation. *Science* **253,** 1325–1326 (1991).
5. Suslick, K. S., Hammerton, D. A. & Cline, R. E. Jr Sonochemical hot spot. *J. Am. Chem. Soc.* **108,** 5641–5642 (1986).
6. Suslick, K. S., Flint, E. B., Grinstaff, M. W. & Kemper, K. A. Sonoluminescence from metal carbonyls. *J. Phys. Chem.* **97,** 3098–3099 (1993).
7. Alkemande, C. T. J., Hollander, T., Snelleman, W. & Zeegers, P. J. T. *Metal Vapours in Flames* (Pergamon, New York, 1982).
8. Wiese, W. L., Fuhr, J. R. & Martin, G. A. Atomic transition probabilities: scandium through manganese. *J. Phys. Chem. Ref. Data* **17,** 311–327 (1988).
9. Wiese, W. L., Fuhr, J. R. & Martin, G. A. Atomic transition probabilities: iron through nickel. *J. Phys. Chem. Ref. Data* **14,** 13–67 (1988).
10. Whaling, W. & Brault, J. W. Comprehensive transition probabilities in molybdenum I. *Phys. Scr.* **38,** 707–715 (1988).
11. Gaydon, A. G. *The Spectroscopy of Flames* 2nd edn (Wiley, New York, 1974).
12. Cabannes, F. & Chapelle, J. in *Reactions Under Plasma Conditions* 1st edn Vol. 1 (ed. Venugopalan, M.) 367–470 (Wiley-Interscience, New York, 1971).
13. Reif, I., Fassel, V. A. & Kniseley, R. N. Spectroscopic flame measurements and their physical significance I: theoretical concepts. *Spectrochim. Acta B* **28,** 105–123 (1973).
14. Jeffries, J. B., Copeland, R. A., Suslick, K. S. & Flint, E. B. Thermal equilibration during cavitation. *Science* **256,** 248 (1992).
15. Noltingk, B. E. & Neppiras, E. Cavitation produced by ultrasonics. *Proc. Phys. Soc. B* **63,** 674–685 (1950).
16. Kamath, V., Prosperetti, A. & Egolfopoulos, F. N. A theoretical study of sonoluminescence. *J. Acoust. Soc. Am.* **94,** 248–260 (1993).
17. Jarman, P. Measurements of sonoluminescence from pure liquids and some aqueous solutions. *Proc. Phys. Soc.* **73,** 628–640 (1959).
18. Flint, E. B. & Suslick, K. S. Sonoluminescence from nonaqueous liquids: emissions from small molecules. *J. Am. Chem. Soc.* **111,** 6987–6992 (1989).
19. Suslick, K. S. & Flint, E. B. Sonoluminescence of alkali metal salts. *J. Phys. Chem.* **95,** 1484–1488 (1991).
20. Suslick, K. S., Gawienowski, J. J., Schubert, P. F. & Wang, H. H. Alkane sonochemistry. *J. Phys. Chem.* **87,** 2299–2301 (1983).
21. Suslick, K. S., Gawienowski, J. W., Schubert, P. F. & Wang, H. H. Sonochemistry in non-aqueous liquids. *Ultrasonics* **22,** 33–36 (1984).
22. Yaws, C. L. *Handbook of Vapor Pressures* Vol. 3, 383 (Gulf, Houston, 1994).
23. Hickling, R. Effects of thermal conduction in sonoluminescence. *J. Acoust. Soc. Am.* **35,** 967–974 (1963).
24. Young, F. R. Sonoluminescence from water containing dissolved gases. *J. Acoust. Soc. Am.* **60,** 100–104 (1976).
25. Yasui, K. *J. Phys. Soc. Jpn* **65,** 2830–2840 (1996).
26. Suslick, K. S. & Flint, E. B. Sonoluminescence of non-aqueous liquids. *Nature* **330,** 553–555 (1987).
27. Zel'dovich, Y. D. & Raizer, Y. P. *Physics of Shock Waves and High Temperature Hydrodynamic Phenomenon* 2nd edn (Academic, New York, 1966).

Acknowledgements

This work was supported by the US National Science Foundation, the US Department of Energy, and in part by the US Defence Advanced Research Projects Agency.

Correspondence and requests for materials should be addressed to K.S.S. (e-mail: ksuslick@uiuc.edu).

Carbon cycling and chronology of climate warming during the Palaeocene/Eocene transition

Richard D Norris* & Ursula Röhl†

* *MS-23, Woods Hole Oceanographic Institution, Woods Hole, Massachusetts 02540-1541, USA*

† *Fachbereich Geowissenschaften, Universität Bremen, Postfach 330 440, 28334 Bremen, Germany*

Current models of the global carbon cycle lack natural mechanisms to explain known large, transient shifts in past records of the stable carbon-isotope ratio ($\delta^{13}C$) of carbon reservoirs[1,2]. The injection into the atmosphere of ~1,200–2,000 gigatons of carbon, as methane from the decomposition of sedimentary methane hydrates, has been proposed to explain a $\delta^{13}C$ anomaly[3,4] associated with high-latitude warming[1] and changes in marine[5–7] and terrestrial[8] biota near the Palaeocene–Eocene boundary, about 55 million years ago. These events may thus be considered as a natural 'experiment' on the effects of transient greenhouse warming. Here we use physical, chemical and spectral analyses of a sediment core from the western North Atlantic Ocean to show that two-thirds of the carbon-isotope anomaly occurred within no more than a few thousand years, indicating that carbon was catastrophically released into the ocean and atmosphere. Both the $\delta^{13}C$ anomaly and biotic changes began between 54.93 and 54.98 million years ago, and are synchronous in oceans and on land. The longevity of the $\delta^{13}C$ anomaly suggests that the residence time of carbon in the Palaeocene global carbon cycle was ~120 thousand years, which is similar to the modelled response after a massive input of methane[3,4]. Our results suggest that large natural perturbations to the global carbon cycle have occurred in the past—probably by abrupt failure of sedimentary carbon reservoirs—at rates that are similar to those induced today by human activity.

The carbon isotope record of marine carbonates is interrupted by a transient negative $\delta^{13}C$ anomaly of −3‰ over an interval of ~100–200 kyr near the end of the Palaeocene[1,9–13]. In the oceans, the $\delta^{13}C$ anomaly is associated with the extinction of 35–50% of cosmopolitan benthic foraminifera[7,10], the appearance of three short-ranging planktic foraminifera[5], a widespread increase in